

Error Performance of Rectangular Pulse-shaped OTFS with Practical Receivers

Cheng Shen, Jinhong Yuan *Fellow, IEEE*, and Hai Lin *Senior Member, IEEE*

Abstract—In this letter, we investigate error performance of rectangular pulse-shaped orthogonal time frequency space (OTFS) modulation with a practical receiver. Specifically, we consider an essential bandpass filter at receiver RF front-end, which has been ignored in existing works. We analyse the effect of rectangular pulses on practical OTFS receiver performance, and derive the exact forms of interference in delay-Doppler (DD) domain. We demonstrate that the transmitted information symbols in certain regions of the DD domain are severely contaminated. As a result, there is an error floor in the receiver error performance, which needs to be addressed for such OTFS waveform in practical systems.

I. INTRODUCTION

AS a 2D modulation technique, orthogonal time frequency space (OTFS) has recently been proposed to combat nasty doubly-selective channels in future communication systems [1], [2]. In OTFS, information is modulated in delay-Doppler (DD) domain and thus coupled with a relatively stable and compact DD domain channel model, which facilitates a simple channel estimation and accurate detection for time-varying channels. This leads to superior performance of OTFS over OFDM when channels are characterised with increasingly larger Doppler spread. It is shown in [1] that if the OTFS transmitter and receiver pulses satisfy the *bi-orthogonality robustness condition* with respect to the time-frequency grid over the support of the channel response, OTFS signals can be detected with a simple one-tap equalizer. However, such pulses are not realizable in practice [1] [3]. Alternatively, one of the most widely investigated OTFS signals was introduced in [3]. It employs a rectangular pulse at the transmitter and receiver to form a signal structure identical to OFDM without slot-wise cyclic prefix (CP), but only adds a single frame-wise CP at the start of an OTFS frame. Compared to CP-based OTFS, which employs a CP for each time slot of the OTFS frame¹, this reduced cyclic prefix (RCP) OTFS scheme has a lower overhead and therefore a higher spectral efficiency. It has become a focal point in OTFS research community, especially for those investigating its practical applications.

A major drawback of rectangular pulse is its high out-of-band emission (OOBE), because the rectangular pulse belongs to the family of time-limited pulses and has a slow-decaying sinc shape in frequency domain. For any practical OFDM systems, OOBE needs to be carefully handled to avoid interference to adjacent channels or self-interference in a band-

limited transmission medium, where the time-limited pulses can lead to severe performance degradation [4].

Since the RCP-OTFS relies on the rectangular pulse based CP-free OFDM through an inverse symplectic finite Fourier transform (ISFFT) precoder, OOBE is also an inevitable practical issue for RCP-OTFS [5]. However, the ISFFT precoder prevents the application of the conventional OOBE suppression approaches adopted in OFDM to the RCP-OTFS. For example, spectral guarding or frequency-domain precoding based OOBE mitigation methods will break the inherent connection between the DD and time-frequency (TF) domain signals governed by the ISFFT precoder. Meanwhile, the absence of CP and cyclic suffix (CS) for each time slot makes windowing based OOBE mitigation methods infeasible, while replacing the rectangular pulse with a spectrally compact pulse leads to severe performance degradation [3], due to loss of orthogonality.

In spite of the importance of OOBE in practical systems, OOBE for RCP-OTFS has not been investigated much in the literature. In particular, existing works on RCP-OTFS assume that without suppressing the OOBE, the transmitted RCP-OTFS waveform is corrupted by the channel dispersion and noise only. However, even the RCP-OTFS signal with high OOBE is allowed to be emitted into the air, the receiver always needs to filter the received signal first. A bandpass filter (BPF) not only prevents the interference and noise from other wireless channels, but also ensures that no aliasing occurs in the subsequent sampling. In other words, a BPF at the receiver's RF front-end is a *must* before all sampling and baseband digital processing operations. Unfortunately, such a vital component is missing in the current modelling and the corresponding analysis of RCP-OTFS, which assumes that the rectangular pulse-shaped RCP-OTFS signal is fully received without bandpass filtering at the receiver, but the noise is restricted to a *narrowband* corresponding to the sampling rate.

In this letter, we study the performance of the rectangular pulse based RCP-OTFS, when the receiver is equipped with a practically necessary BPF. We show that with BPF, the transmitted DD domain symbols of rectangular pulse-shaped OTFS shift away from their initial constellation point and suffers from interference from other DD domain symbols. We shall point out that such interference is due to the rectangular pulse and BPF, which is different from the interference analysed in previous work such as [7], which is caused by the channel dispersion. Our further analysis shows that the bandpass filtered waveform experiences an unevenly distributed distortion across the DD grid, and demonstrates that the distortion introduces severe error floor for the OTFS error performance with a message passing detector.

Manuscript received April 1, 2022; revised August 16, 2022.

¹The CP-based OTFS can be interpreted as pre-processed OFDM and implemented as an overlay to existing OFDM systems [1], [2].

II. OTFS SYSTEM MODEL

In an OTFS transmitter, symbols $X[k, l]$ from a complex signal constellation are mapped to a DD domain grid, with $k \in \{0, 1, \dots, N-1\}$ and $l \in \{0, 1, \dots, M-1\}$ representing their Doppler and delay indices, respectively. The signal is then converted to TF domain by applying an ISFFT [1]

$$\mathcal{X}[n, m] = \frac{1}{\sqrt{MN}} \sum_{k=0}^{N-1} \sum_{l=0}^{M-1} X[k, l] e^{j2\pi(\frac{nk}{N} - \frac{ml}{M})}, \quad (1)$$

where $m \in \{0, 1, \dots, M-1\}$ indicates the frequency index and $n \in \{0, 1, \dots, N-1\}$ represents the time index. The TF domain form of the signal is equivalent to N OFDM symbols with M subcarriers. Orthogonality is achieved when the subcarrier spacing Δf and OFDM symbol duration T adheres to the relationship $\Delta f = \frac{1}{T}$. Next, the Heisenberg transform is performed to yield the time domain signal [1]

$$s(t) = \sum_{n=0}^{N-1} \sum_{m=0}^{M-1} \mathcal{X}[n, m] e^{j2\pi m \Delta f (t - nT)} g_{tx}(t - nT), \quad (2)$$

where $g_{tx}(t)$ defines the OFDM symbol-wise pulse shape at transmitter. Frame-wise CP of length L -sample is added, corresponding to extending the time span of the signal to $[-L\frac{T}{M}, NT]$, such that $L\frac{T}{M}$ is longer than the estimated channel delay spread [2].

When the signal is passed through a time-frequency dispersion channel, the received signal is given by

$$r(t) = \int \int a(\tau, \nu) e^{j2\pi\nu(t-\tau)} s(t-\tau) d\tau d\nu + w(t), \quad (3)$$

where $a(\tau, \nu)$ denotes the spreading function of the channel and $w(t)$ denotes AWGN. It is further assumed that the equivalent sampling channel, representing the physical channel subject to the delay-Doppler resolution $\{\frac{T}{M}, \frac{1}{NT}\}$, has P paths on the DD grid, which leads to [6]

$$a(\tau, \nu) = \sum_{i=1}^P a_i \delta(\tau - \tau_i) \delta(\nu - \nu_i), \quad (4)$$

where δ denotes Dirac Delta, a_i is the path gain, τ_i is the delay as an integer multiple of $\frac{1}{M\Delta f}$, and ν_i is the Doppler as an integer multiple of $\frac{1}{NT}$ of the i th path.

The receiver performs Wigner transform on $r(t)$ followed by sampling, yielding the discrete TF domain signal [2].

$$\mathcal{Y}[n, m] = \int g_{rx}^*(t' - t) r(t') e^{-j2\pi f(t' - t)} dt' \Big|_{t=nT, f=m\Delta f}, \quad (5)$$

where $g_{rx}(t)$ is the receiver pulse. For rectangular pulse shape,

$$g_{tx}(t) = g_{rx}(t) = \begin{cases} 1 & 0 \leq t \leq T, \\ 0 & \text{otherwise.} \end{cases}$$

Note that the process in (5) is equivalent to first sampling in time domain and doing all transforms in a discrete form, as is performed by a practical receiver. Finally, the TF domain received signal is transformed to DD domain via symplectic finite fourier transform (SFFT),

$$Y[k, l] = \frac{1}{\sqrt{NM}} \sum_{n=0}^{N-1} \sum_{m=0}^{M-1} \mathcal{Y}[n, m] e^{-j2\pi(\frac{nk}{N} - \frac{ml}{M})},$$

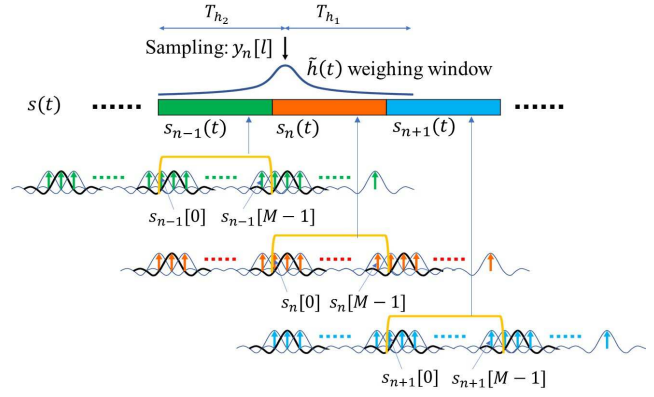


Fig. 1. The equivalent process of Heisenberg Transform and effect of filtering on OTFS signals. The yellow window indicates the per-OFDM pulse $g_{tx}(t)$. $\hat{h}(t) = h(-t)$ represents the mirror image of $h(t)$

where detection is performed.

III. INTERFERENCE ANALYSIS

A. Interference in discrete time domain

At the transmitter, the MN discrete time domain samples of N OFDM symbols in an OTFS frame can be given by

$$s[nM + l] = \sum_{m=0}^{M-1} \mathcal{X}[n, m] e^{j\frac{2\pi ml}{M}}, \quad (6)$$

with $0 \leq n \leq N-1$ and $0 \leq l \leq M-1$. Then, for the n th OFDM symbol (the n th time slot), we have M samples $\mathbf{s}_n = [s[nM], \dots, s[nM + M-1]]$. Combining the ISFFT in (1) and the IDFT in (6), the l th element of \mathbf{s}_n can be obtained from the inverse discrete Zak transform as

$$s_n[l] = s[nM + l] = \frac{1}{\sqrt{N}} \sum_{k=0}^{N-1} X[k, l] e^{j\frac{2\pi nk}{N}}. \quad (7)$$

For ease of analysis, we rewrite the transmitted signal $s(t)$ in (2) into a form which is interpolated and windowed from MN samples in (6). The process is also shown in the lower part of Fig. 1. Let $(\cdot)_M$ denotes modulo M , assuming a T -duration frame-wise CP, the OTFS frame can be written as

$$s(t) = \sum_{n=-1}^N s_n(t)$$

where the n th T -duration slot is

$$s_n(t) = g_{tx}(t - nT) \sum_{l'=-\infty}^{\infty} s_n[(l')_M] \text{sinc}\left(t - l' \frac{T}{M} - nT\right), \quad (8)$$

for $0 \leq n \leq N-1$, while $s_{-1}(t) = s_{N-1}(t + NT)$ and $s_N(t) = 0$ correspond to the frame-wise CP and the frame termination, respectively. Obviously, because of $g_{tx}(t) = 0$ for $t \notin [0, T]$, we have $s_n(t) = 0$ for $t \notin [nT, (n+1)T]$.

The main focus of the letter is to analyse the rectangular pulse's effect on OTFS's receiver performance. To provide some insight and simplify tedious analysis, we consider the AWGN channel with a spread function $a(\tau, \nu) = \delta(\tau)\delta(\nu)$ and temporarily ignore the noise. In that case, the received

signal at the RF front-end is identical to the transmitted signal, namely, $r(t) = s(t)$ except that a BPF is applied to $r(t)$ before sampling. Considering the AWGN channel means that the receiver performance is solely affected by the rectangular pulse with BPF and not by the channel dispersion. In Section IV, we will also show the OTFS performance over practical doubly-selective channels.

Now we consider the BPF of the practical receiver. Ideally, the bandwidth of this BPF should be just enough to pass the signal, while rejecting as much noise as possible from the band where spectral component of the signal is insignificant. We assume that the lowpass equivalent of the BPF, referred to as LPF from hereon, is a non-causal filter with its impulse response $h(t)$ supported on $[-T_{h1}, T_{h2}]$ and peaks at $t = 0$. This ensures that equivalent sampling at receiver could be made at integer multiples of $\frac{T}{M}$, and change of the LPF causality only introduces a group delay that can be equalized easily. Then, let \mathbf{y} denote the discrete time samples of the filtered receiver signal and $\mathbf{y}_n = [y[nM], \dots, y[nM + M - 1]]$ denote the samples in the n th time slot of \mathbf{y} , we have

$$\begin{aligned} y_n[l] &:= y[nM + l] = r(t) * h(t)|_{t=nT+l\frac{T}{M}} \\ &= \int h\left(nT + l\frac{T}{M} - t'\right) s(t') dt', \end{aligned} \quad (9)$$

where $0 \leq n \leq N - 1$, $0 \leq l \leq M - 1$, and $*$ denotes convolution. The effect of filtering on the OTFS signal is shown in Fig. 1. It can be seen that the integration in (9) includes signals spanned by the discrete samples in the preceding, current and succeeding slots, which introduces interference.

In the following interference analysis, we consider the practical case where the impulse response of the LPF is shorter than the slot length, namely, $T_{h1}, T_{h2} < T$. Recall that $s_n(t) = 0$ for $t \notin [nT, (n+1)T]$, (9) can be simplified as

$$y_n[l] = \sum_{q=-1}^1 \underbrace{\int_{(n+q)T}^{(n+q+1)T} h\left(nT + l\frac{T}{M} - t'\right) s_{n+q}(t') dt'}_{y_n^{(q)}[l]},$$

where $y_n^{(q)}[l]$ denotes the signal received at the l th delay position in the n th time slot due to the contribution from the preceding, current and succeeding slots when $q = -1, 0, 1$, respectively. Substituting (8) into $y_n^{(q)}[l]$, we obtain

$$\begin{aligned} y_n^{(q)}[l] &= \sum_{l'=-\infty}^{\infty} s_{n+q}[(l')_M] \times \\ &\quad \underbrace{\int_{qT}^{(q+1)T} h\left(l\frac{T}{M} - t'\right) \text{sinc}\left(t' - l'\frac{T}{M}\right) dt'}_{i^{(q)}[l, l']} \end{aligned} \quad (10)$$

where $i^{(q)}[l, l']$ represents the level of interference caused by the l' th discrete time symbol from the preceding, current and succeeding slots on the l th discrete time symbol in the current slot, for $q = -1, 0, 1$, respectively.

If $s(t)$ is a strictly band-limited signal without OOBE, the receiver LPF would not change the signal and hence introduces

no interference. In that case, we have the orthogonality between the sample-wise transmitting pulse and the LPF impulse response [4]

$$\int_{-\infty}^{\infty} h\left(l\frac{T}{M} - t'\right) \text{sinc}\left(t' - l'\frac{T}{M}\right) dt' = \delta[l - l'], \quad (11)$$

which is analogous to Nyquist Criterion for pulses. Note that this orthogonality holds only when the entire support of sinc and $h(t)$ is included in the integration. Unfortunately, the rectangular pulse of OTFS breaks the integrity of integration range and results in non-trivial values of $i^{(q)}[l, l']$.

B. Interference analysis in DD domain

The received signal and interference can be analysed in the DD domain by performing a discrete Zak Transform on the MN time domain discrete samples from (9). First, let us represent l' in (10) as $l' = l_2M + l_1$, with $0 \leq l_1 \leq M - 1$ and $-\infty < l_2 < \infty$. For a given q , we then have

$$\begin{aligned} y_n^{(q)}[l] &= \sum_{l_1=0}^{M-1} \sum_{l_2=-\infty}^{\infty} s_{n+q}[l_1] i^{(q)}[l, l_2M + l_1] \\ &= \sum_{l_1=0}^{M-1} s_{n+q}[l_1] \underbrace{\sum_{l_2=-\infty}^{\infty} i^{(q)}[l, l_2M + l_1]}_{I^{(q)}[l, l_1]}, \end{aligned} \quad (12)$$

where $I^{(q)}[l, l_1]$ represents the level of interference caused by the l_1 -th discrete time symbol from the preceding ($q = -1$), current ($q = 0$) and succeeding ($q = 1$) slots on the l th discrete time symbol in the current slot, respectively, where $l \in \{0, 1, \dots, M - 1\}$ and $l_1 \in \{0, 1, \dots, M - 1\}$. From hereon, we use the time delay representation for the transmitted and receiver signals as $s[n, l] = s_n[l]$ and $y[n, l] = y_n[l]$, where $0 \leq n \leq N - 1$ denotes the time index and $0 \leq l \leq M - 1$ denotes the delay index. The DD domain discrete samples can thus be given by

$$Y[k, l] = \frac{1}{\sqrt{N}} \sum_{n=0}^{N-1} y[n, l] e^{-j2\pi \frac{nk}{N}} \quad (13)$$

$$= \sum_{l_1=0}^{M-1} \left(\sum_{q=-1}^1 I^{(q)}[l, l_1] \left\{ \frac{1}{\sqrt{N}} \sum_{n=0}^{N-1} (s[n+q, l_1]) e^{-j2\pi \frac{nk}{N}} \right\} \right).$$

By (5), for any delay index l_1 , the DFT of $s[n, l_1]$ yields exactly $X[k, l_1]$, while $s[n-1, l_1] = s[(n-1)_N, l_1]$ and $s[n+1, l_1] = s[(n+1)_N, l_1] + s_c[n, l_1]$ for $n = 0, 1, \dots, N - 1$, where

$$s_c[n, l_1] = \begin{cases} 0 & n = 0, 1, \dots, N - 2 \\ -\frac{1}{\sqrt{N}} \sum_{k=0}^{N-1} X[k, l_1] & n = N - 1 \end{cases}$$

Now let us analyse (13). Since a cyclic shift in time domain corresponds to linear phase variation in discrete Doppler domain, for any l_1 , we have

$$\begin{aligned} Y[k, l] &= \sum_{l_1=0}^{M-1} \left(\sum_{q=-1}^1 I^{(q)}[l, l_1] X[k, l_1] e^{\frac{j2\pi k}{N} q} \right. \\ &\quad \left. - I^{(1)}[l, l_1] \left(\frac{1}{N} \sum_{k'=0}^{N-1} X[k', l_1] \right) e^{-\frac{j2\pi k(N-1)}{N}} \right) \end{aligned} \quad (14)$$

and hence,

$$Y[k, l] = C[k, l]X[k, l] + \underbrace{\sum_{(k', l_1) \neq (k, l)} C[k', l, l_1]X[k', l_1]}_{I[k, l]} \quad (15)$$

for $k' \in \{0, 1, \dots, N-1\}$ and $l_1 \in \{0, 1, \dots, M-1\}$, where

$$C[k', l, l_1] = \begin{cases} I^{(0)}[l, l_1] + I^{(-1)}[l, l_1]e^{-\frac{j2\pi k}{N}} \\ \quad + I^{(1)}[l, l_1] \left(e^{\frac{j2\pi k}{N}} - \frac{1}{N}e^{-\frac{j2\pi k(N-1)}{N}} \right), & k' = k \\ -\frac{1}{N}I^{(1)}[l, l_1]e^{-\frac{j2\pi k'(N-1)}{N}}, & k' \neq k \end{cases} \quad (16)$$

The first term in (15) denotes the desired signal received on the $[k, l]$ -th DD grid, scaled by a complex coefficient $C[k, l]$, which represents the amplitude change and phase rotation for the transmitted symbol on the same grid. On the other hand, the second term of (15) stands for interference from symbols transmitted on all the grid points in DD domain with $(k', l_1) \neq (k, l)$. Hence, we define $I[k, l]$ as inter-delay-Doppler-interference (IDDI) for the symbol on the $[k, l]$ -th DD grid. Note that it is a linear combination of *i.i.d* variables $X[k', l_1]$ with zero mean and variance σ_s^2 , where σ_s^2 is the average symbol energy of $X[k, l]$. Thus, the average IDDI power is given by

$$\begin{aligned} V[k, l] &= \mathbb{E} \{ I[k, l] \cdot I^*[k, l] \} \\ &= \mathbb{E} \{ X[k, l] \cdot X^*[k, l] \} \sum_{(k', l_1) \neq (k, l)} C[k', l, l_1] C^*[k', l, l_1] \\ &= \sigma_s^2 \sum_{\substack{l_1 \neq l, \\ l_1=0}}^{M-1} |C[k, l, l_1]|^2 + \frac{\sigma_s^2(N-1)}{N^2} \sum_{l_1=0}^{M-1} \left(I^{(1)}[l, l_1] \right)^2, \end{aligned} \quad (17)$$

which shows its relation to k , l and $h(t)$. The signal to interference power ratio (SIR) on each (k, l) DD grid, without considering the interference caused by the channel dispersion, can thus be quantitatively calculated as

$$\text{SIR}[k, l] = \frac{\sigma_s^2 |C[k, l, l]|^2}{V[k, l]}. \quad (18)$$

IV. INTERFERENCE AND PERFORMANCE EVALUATION

In this section, the derivation of expected interference power from Section III is verified and compared with simulation, and error performance of the rectangular pulse shaped RCP-OTFS is evaluated for both the AWGN and doubly-selective channels. In our simulation, the LPF is a near-rectangular filter with a bandwidth $\frac{M}{T}$ and its time response is a truncated sinc which centres at $t = 0$ and $T_{h_1} = T_{h_2} = T$. Other types of LPFs, such as Bessel, Chebyshev and Butterworth filters, etc., will have similar effect.

In Figs. 2 to 4, we demonstrate the effect of rectangular pulse and filtering by showing the amplitude and phase changes of signal component and interference on different DD grids in the AWGN channel. We use $M = 128$ and $N = 16$

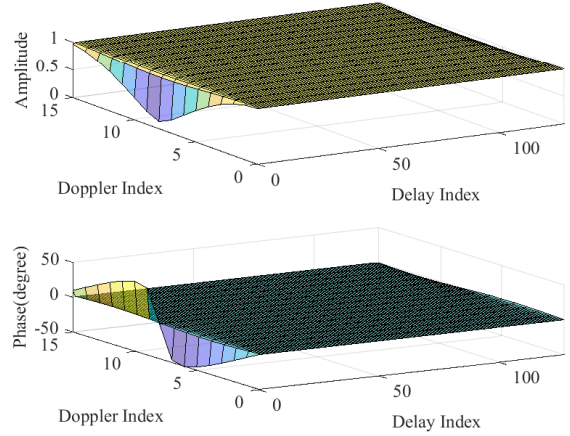


Fig. 2. Amplitude and phase variation for the transmitted DD domain signals

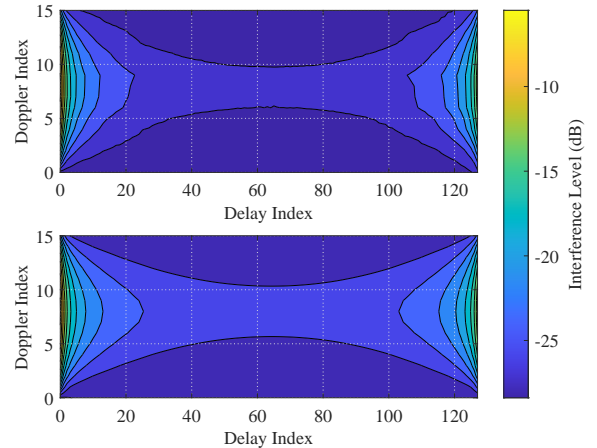


Fig. 3. Average interference power on delay-Doppler domain grid: (a) upper sub-figure: simulation result (b) lower sub-figure: derivation results from (17)

as an example, which provides better visibility of interfered region in the figures. Fig. 2 shows the amplitude change and phase rotation experienced by the transmitted DD domain symbols, described by $C[k, l, l]$ in (16). For most symbols, $C[k, l, l]$ is approximately a unity-length, zero-phase vector, which corresponding to almost no shift of the transmitted signal. Nonetheless, attenuation in power can be observed for symbols with delay index close to zero or M while Doppler index k is close to $\frac{N}{2}$. This is due to relatively large values of $I^{(-1)}[l, l]$ when l approaches zero and large values of $I^{(1)}[l, l]$ when l approaches M . When k is around $\frac{N}{2}$, $I^{(-1)}[l, l]e^{-\frac{j2\pi k}{N}}$ and $I^{(1)}[l, l]e^{\frac{j2\pi k}{N}}$ are in opposite direction to the desired signal in the signal space, resulting in significant decrease of the original signal power.

A description of average IDDI power and its variation with delay and Doppler indices is shown in Fig. 3. The upper sub-figure presents the average interference power measured from simulation and the lower one is a plot of derivation result in (17). It can be seen that the estimated IDDI power agrees with the measurement from simulation. The contours of interference

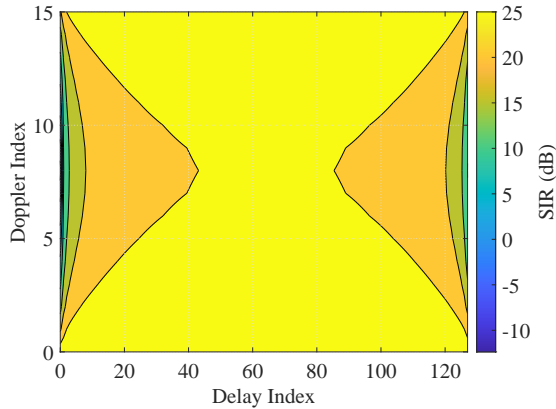


Fig. 4. SIR on delay-Doppler domain grid

level is of hyperbola-like shape. Severe interference will be experienced by a symbol when its delay index is closer to 0 or $M - 1$, and its Doppler index is closer to $N/2$. The SIR on each delay-Doppler grid is shown in Fig. 4, which follows a similar shape. Note that SIR is below 0 dB with Doppler index k close to $\frac{N}{2}$ and delay index l closer to 0, which will dominate system performance when SNR is high.

The bit error rate (BER) performance of the OTFS system in the AWGN and doubly-selective channels is presented in Fig. 5, where $E_s = \sigma_s^2$ and N_0 is power spectral density of AWGN. DD domain 4-QAM symbols are employed to carry information. The message passing (MP) algorithm from [7] is used for data detection. The nodes connection in the factor graph of the MP algorithm is governed by the input-output relationship for rectangular pulse-shaped OTFS given by Equation (24) in [7], which is widely accepted yet has not considered the effect of BPF. Moreover, for the “ideal” cases in Fig. 5, we assume that the theoretically band-unlimited rectangular pulse-shaped RCP-OTFS is fully received without BPF, while the AWGN is restricted to a bandwidth of $\frac{M}{T}$. Note that such an ideal assumption is not realizable in practice.

In the AWGN channel, we can see from Fig. 5 that for the rectangular pulse-shaped OTFS system with ($M = 128, N = 16$) and a practical receiver, an error floor occurs at BER around 10^{-3} when $E_s/N_0 \geq 13$ dB, while there is no error floor in the ideal case without BPF. Simulation results with other frame sizes of ($M = 512, N = 16$) and ($M = 128, N = 32$) are also plotted for comparison. It can be noticed that there is also an error floor but occurs at a lower BER when M increases. This is because of a relatively smaller proportion of interfered region in the entire frame for a larger M . Furthermore, we observe that no performance change occurs when N varies. For practical channels, we choose $M = 512$ and $N = 32$ and use the Extended Vehicular A (EVA) model [8] as the delay profile. Doppler for each path is generated randomly with Jakes’ formula [9] under the assumptions that $\Delta f = 15$ kHz, carrier frequency $f_c = 5$ GHz and maximum relative speed $v_{max} = 120$ km/h. Again, the BER curve for practical receiver touches the error floor at BER slightly below 10^{-3} , which is not observed in the ideal case. Similar effect on error performance can also be observed

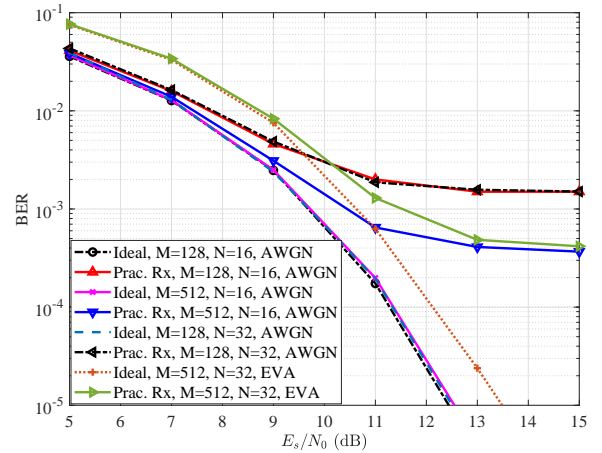


Fig. 5. BER performance of rectangular pulse-shaped RCP-OTFS. For the MP algorithm, damping factor is 0.7, and maximum iteration number is 50.

for higher order modulations, which is not shown due to space limitation.

V. CONCLUSION

In this letter, we investigate the effect of rectangular pulse-shaping on error performance of OTFS modulation for practical receiver with a BPF. Assuming OOB not handled, we first show that the rectangular pulse can introduce time domain interference for RCP-OTFS when band-limitation is applied. In DD domain, such interference corresponds to amplitude change and phase rotation of transmitted symbols as well as inter-delay-Doppler interference, the formula for which are derived. Our analysis shows that symbols mapped to the edges of delay and the middle of Doppler on the DD grid are most severely corrupted. Finally, error performance for such waveform is evaluated for both AWGN and doubly-selective channels, where an error floor can be observed at high SNRs.

REFERENCES

- [1] R. Hadani, S. Rakib, M. Tsatsanis, A. Monk, A. J. Goldsmith, A. F. Molisch, and R. Calderbank, “Orthogonal time frequency space modulation,” in *Proc. of IEEE WCNC*, 2017.
- [2] R. Hadani, S. Rakib, S. Kons, M. Tsatsanis, A. Monk, C. Ibars, J. Delfeld, Y. Hebron, A. J. Goldsmith, A. F. Molisch, and R. Calderbank, “Orthogonal time frequency space modulation,” 2018, arXiv:1808.00519.
- [3] P. Raviteja, Y. Hong, E. Viterbo, and E. Biglieri, “Practical pulse-shaping waveforms for reduced-cyclic-prefix OTFS,” *IEEE Trans. Veh. Technol.*, vol. 68, no. 1, pp. 957–961, 2019.
- [4] R. W. Chang, “Synthesis of band-limited orthogonal signal for multi-channel data transmission,” *Bell Syst. Tech. J.*, vol. 45, no. 10, pp. 1775–1796, 1966.
- [5] H. Lin and J. Yuan, “Orthogonal delay-Doppler division multiplexing modulation,” *IEEE Trans. Wireless Commun.*, 2022, to appear.
- [6] P. Bello, “Characterization of randomly time-variant linear channels,” *IEEE Trans. Commun. Syst.*, vol. 11, no. 4, pp. 360–393, 1963.
- [7] P. Raviteja, K. T. Phan, Y. Hong, and E. Viterbo, “Interference cancellation and iterative detection for orthogonal time frequency space modulation,” *IEEE Trans. Wireless Commun.*, vol. 17, no. 10, pp. 6501–6515, 2018.
- [8] “Evolved universal terrestrial radio access (e-utra); user equipment (ue) radio transmission and reception,” 3GPP TS 36.101; 3rd Generation Partnership Project; Technical Specification Group Radio Access Network, Tech. Rep., 2016.
- [9] W. Jakes, *Microwave Mobile Communications*. New York, NY, USA: Wiley, 1974.